



# Development of the Alpha Rhythm Is Linked to Visual White Matter Pathways and Visual Detection Performance

 Sedy Caffarra,<sup>1,2,3</sup> Klint Kanopka,<sup>2</sup> John Kruper,<sup>4,5</sup> Adam Richie-Halford,<sup>1,2</sup> Ethan Roy,<sup>2</sup>  Ariel Rokem,<sup>4,5</sup> and Jason D. Yeatman<sup>1,2</sup>

<sup>1</sup>Division of Developmental-Behavioral Pediatrics, Stanford University School of Medicine, Stanford 94305, California, <sup>2</sup>Stanford University Graduate School of Education, Stanford 94305, California, <sup>3</sup>Department of Biomedical, Metabolic and Neural Sciences, University of Modena and Reggio Emilia, Modena 41125, Italy, <sup>4</sup>Department of Psychology, University of Washington, Seattle 91905, Washington, and <sup>5</sup>eScience Institute, University of Washington, Seattle 98195-1570, Washington

Alpha is the strongest electrophysiological rhythm in awake humans at rest. Despite its predominance in the EEG signal, large variations can be observed in alpha properties during development, with an increase in alpha frequency over childhood and adulthood. Here, we tested the hypothesis that these changes in alpha rhythm are related to the maturation of visual white matter pathways. We capitalized on a large diffusion MRI (dMRI)-EEG dataset (dMRI  $n = 2,747$ , EEG  $n = 2,561$ ) of children and adolescents of either sex (age range, 5–21 years old) and showed that maturation of the optic radiation specifically accounts for developmental changes of alpha frequency. Behavioral analyses also confirmed that variations of alpha frequency are related to maturational changes in visual perception. The present findings demonstrate the close link between developmental variations in white matter tissue properties, electrophysiological responses, and behavior.

**Key words:** alpha; development; dMRI; EEG; vision

## Significance Statement

The present work shows that the maturation of visual white matter pathways (optic radiations) specifically accounts for the developmental increase of brain oscillation frequency (alpha), which is ultimately related to an enhancement of visual perception during childhood and adolescence. The present findings are an example of how relating white matter properties to functional aspects of the brain can help us reach a more complete understanding of the link between the development of brain connectivity, changes in electrophysiology, and visual perception.

## Introduction

The alpha rhythm (8–12 Hz) is one of the most prominent and consistent electrophysiological signatures in both human and animal brains (Berger, 1938; Lopes Da Silva and Storm Van Leeuwen, 1977; Popov and Szyszka, 2020). In the 1920s, this dominant brain rhythm was first reported in humans at rest by Hans Berger. Despite its widespread occurrence and long history, the neuroanatomical structures that influence the alpha rhythm

and its development are still under discussion. This work capitalizes on structural [diffusion magnetic resonance imaging (dMRI)] and functional [electroencephalography (EEG)] brain measures from a large sample (dMRI = 2,747, EEG = 2,561) spanning 5–21 years of age to clarify the neurobiological underpinnings of human spontaneous alpha across development.

One of the major neural sources of the human alpha rhythm is the thalamus [pulvinar and lateral geniculate nucleus (LGN); Hughes and Crunelli, 2005; Lorincz et al., 2009; Vijayan and Kopell, 2012], whose crucial role has been shown in *in vitro* slice preparations (Hughes et al., 2004) and further confirmed by human studies where fluctuations in thalamic activity (due to tasks or lesions) lead to changes in occipital alpha (Lukashevich and Sazonova, 1996; Goldman et al., 2002; Liu et al., 2012). Besides the thalamus, additional alpha generators have been localized in the visual cortex of both humans and animals (Lopes Da Silva and Storm Van Leeuwen, 1977; Lopes da Silva, 1991; Traub et al., 2020). Crucially, these thalamic and cortical generators can synchronize. This neural synchronization modulates the EEG

Received April 14, 2023; revised Nov. 21, 2023; accepted Nov. 29, 2023.

Author contributions: S.C. and J.D.Y. designed research; S.C., K.K., J.K., A.R.-H., E.R., A.R., and J.D.Y. performed research; S.C., K.K., J.K., A.R.-H., E.R., A.R., and J.D.Y. analyzed data; S.C. wrote the paper.

This project has received funding from the European Union's Horizon 2020 research and innovation program under the Marie Skłodowska-Curie Grant Agreement No. 837228, FAR2022INTERM\_O\_UNIM, P2022SMEJW, and Italian Ministry of University and Research Rita Levi Montalcini to S.C. This work was also supported by NSF/BSF BCS #1551330, NICHD R01HD09586101, NICHD R21HD092771 and Jacobs Foundation Research Fellowship to J.D.Y. and NIH RF1MH121868-01 to A.R. and J.D.Y.

The authors declare no competing financial interests.

Correspondence should be addressed to Sedy Caffarra at caffarra@stanford.edu.

<https://doi.org/10.1523/JNEUROSCI.0684-23.2023>

Copyright © 2024 the authors

signal recorded on the scalp (Musall et al., 2014) and shows a high degree of alpha coherence (Lopes da Silva et al., 1973, 1980). This supports the idea that modulations of alpha depend not only on a single brain area's activity but also on corticothalamic connections (Halgren et al., 2019) and their white matter properties (Nunez et al., 2015). Specifically, mathematical models of spontaneous brain rhythms have proposed that electrophysiological oscillations can be described as a function of the structural properties of white matter fibers (e.g., fiber length and myelination; Jirsa and Haken, 1996, 1997; Nunez, 2011). Moreover, the white matter architecture has been argued to be specifically constraining for the dynamics of alpha rhythm (Valdés-Hernández et al., 2010; Hindriks et al., 2015; Minami et al., 2020). Despite the high precision of these models, there is still no definitive evidence supporting the theorized link between white matter and alpha. Optic radiation has been the most studied corticothalamic pathway since it connects two major alpha generators: LGN and the primary visual cortex (Sherbondy et al., 2008). However, the experimental findings are mixed, with research studies reporting positive effects (Hindriks et al., 2015; Minami et al., 2020; Tröndle et al., 2022), null effects (Renauld et al., 2016) and studies implicating other cortical connections (Valdés-Hernández et al., 2010). Some of these inconsistencies likely stem from heterogeneous EEG-dMRI analysis pipelines across studies and small sample sizes (most previous studies included 10–30 participants; Hindriks et al., 2015; Renauld et al., 2016; Minami et al., 2020).

The present work leverages a large EEG-dMRI dataset including children and adults ranging from 5 to 21 years of age and reveals a relationship between white matter fiber properties and individual differences in spontaneous alpha activity. This structural–functional link is specific to the optic radiation and is consistent across development. Biophysical modeling of the diffusion signal suggests that the structural–functional link is driven by individual differences in axon water fraction (AWF) within the optic radiations. Moreover, developmental changes of alpha are partially mediated by the development of optic radiation. Additional analyses on potential behavioral correlates of alpha confirmed its role in the accuracy of visual target detection (Van Dijk et al., 2008; Mathewson et al., 2009; Samaha and Postle, 2015; Di Gregorio et al., 2022). This is in line with the idea that the alpha rhythm reflects a general brain mechanism of inhibition that modulates visual processing by selectively gating the neural signal flow between the thalamus and V1 (Jensen and Mazaheri, 2010; Jensen et al., 2014, 2021). These findings reveal a link between the development of visual white matter pathways, brain oscillations, and visual behavior.

## Materials and Methods

**Participants.** Data of participants came from the Healthy Brain Network (HBN) pediatric mental health study (Alexander et al., 2017), which included dMRI (initial raw data sample size = 2,747) and EEG (initial raw data sample size = 2,561) measures of English-speaking children and adolescents of either sex from 5 to 21 years of age. The exclusion criteria included moderate to severe cognitive impairment (IQ below 65), encephalopathy, neurodegenerative disorders, hearing, and visual impairment. All participants had normal or corrected-to-normal vision. Informed consent was obtained for each participant above 18 years of age. Written assent was obtained for younger participants, and their legal guardians were asked to sign a written consent.

**dMRI acquisition and preprocessing.** Diffusion MRI (dMRI) data were acquired using a 1.5 T Siemens mobile scanner and three fixed 3 T Siemens scanners in the New York area (four locations: Staten Island, Rutgers University Brain Imaging Center, CitiGroup Cornell

Brain Imaging Center, and City University of New York Advanced Science Research Center). Voxel resolution was  $1.8 \times 1.8 \times 1.8$  mm with 64 noncollinear directions measured for each of  $b = 1,000$  s/mm<sup>2</sup> and  $b = 2,000$  s/mm<sup>2</sup>.

QSIprep (Cieslak et al., 2021) preprocessed dMRI data were accessed from AWS S3 at `s3://fcp-indi/data/Projects/HBN/BIDS_curated/derivatives/qsiprep/` together with individual quality control scores ( $n = 1,885$ ; for the preprocessing pipeline description and quality control scores definition, see Richie-Halford et al., 2022b). The left and the right optic radiations were identified using pyAFQ (Krupar et al., 2021) based on two endpoint regions of interest [ROIs; for a similar pipeline see, Caffarra et al., (2021)]: the primary visual cortex and the central part of the thalamus including the LGN (defined based on the AICHA atlas, minimum distance 3 mm; Joliot et al., 2015). Three exclusion ROIs were also used to further clean the tract from crossing fibers (temporal pole and occipital pole from the AICHA atlas and the posterior portion of the thalamus based on the Brainnetome Atlas; minimum distance 3 mm; Sherbondy et al., 2008; Fan et al., 2016). All ROIs were defined in an MNI template and transformed to each participant's native space based on a nonlinear registration between the template and individual brain anatomy (Avants et al., 2008). A final cleaning step was carried out to remove outlier fibers based on streamlined average length and mean Gaussian distance from the bundle core (distance threshold, 3 mm; length threshold, 4 SD; Yeatman et al., 2012). Diffusion metrics were calculated using the diffusion kurtosis model (DKI; Jensen et al., 2005; Henriques et al., 2021) projected onto the optic radiations, and fractional anisotropy (FA), mean diffusivity (MD), and axonal water fraction (AWF) were mapped onto each tract, weighting the values based on the streamline's distance from the core of the tract (Yeatman et al., 2012). Overall, we could detect the left optic radiations in 1,798 participants and the right optic radiations in 1,799 participants. Further analysis was conducted only on participants where both left and right optic radiation could be found ( $n = 1,774$ ). FA, MD, and AWF values of the left and right optic radiations were averaged for each participant. Moreover, the mean length of the optic radiations was calculated by averaging the median values of the streamline length for the left and right optic radiations (step size = 0.5 mm). A similar pyAFQ pipeline was used for other default white matter bundles (total, 24), among which a subset of corticothalamic (anterior thalamic radiation and corticospinal tract) and posterior bundles (inferior fronto-occipital fascicle, occipital and posterior parietal part of the corpus callosum) were used as control tracts. Only participants with quality control scores higher than 0.3 (based on Richie-Halford et al., 2022a) were included in the final statistical analyses (final dMRI sample size = 1,394; Fig. 1).

**EEG acquisition and preprocessing.** EEG data were recorded with a 128-channel EEG geodesic hydrocele (Magstim EGI) in a sound-shielded room of one of the four New York recording locations (sampling rate = 500 Hz; bandpass filter = 0.1–100 Hz). The online reference was at Cz.

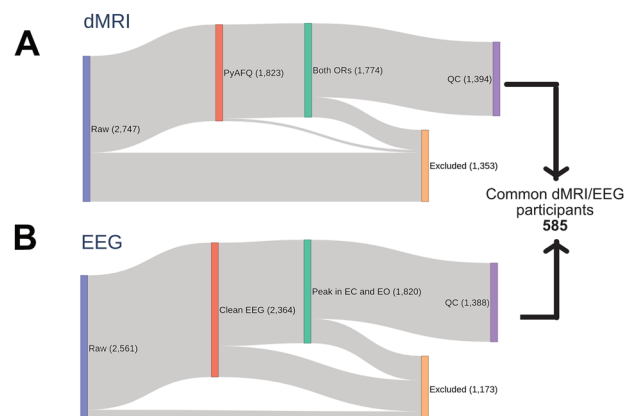


**Figure 1.** Graphical representation of the participant selection process.

The impedance was kept below 40 kOhm and tested every 30 min of EEG recording. EEG raw data were accessed from <s3://fcp-indi/data/Projects/HBN/EEG>.

EEG analysis was performed on a cluster of 13 occipital electrodes (E69, E70, E71, E72, E73, E74, E75, E76, E81, E82, E83, E88, E89) using MNE (Gramfort et al., 2013). The EEG signal was re-referenced offline to the mastoids' average activity. High and low pass filters were applied (1 and 40 Hz, respectively). Epochs of 10 s were segmented for each condition [total of 10 epochs, 5 for eyes closed (EC) and 5 for eyes open (EO) condition]. Bad EEG epochs were automatically rejected or corrected by using the autoreject algorithm (Jas et al., 2017), which has been already employed for the preprocessing of the big electrophysiological dataset (Human Connectome Project, Van Essen et al., 2013; Jas et al., 2017). Having an additional preprocessing step where ocular artifacts were further corrected through ICA did not affect the structural-functional results reported here. Only participants with at least two clean epochs for EC and EO (minimum duration of clean EEG signal = 20 s) were further analyzed ( $n = 2,364$ ). A trial-by-trial time frequency analysis was performed using a multitaper estimation of the power spectra (Altis, 1996) and then averaged across epochs and electrodes of the cluster (the multitaper was chosen as it has been reported to have the highest signal-to-noise ratio compared to other spectral decomposition methods; Lendner et al., 2020). The power spectrum was estimated from 1 to 40 Hz, with a window half-bandwidth of 4 Hz. We used the Fitting Oscillations and One-Over-F (FOOOF) toolbox (Donoghue et al., 2020b) to estimate the periodic and aperiodic signals of each individual power spectrum (peak width = 0.5–20; maximum oscillatory peaks = 1; minimum peak height = 0.2). Most of the participants had a maximum power peak of ~10 Hz in both EC and EO conditions (Fig. 2). Only those participants that showed a maximum oscillatory peak in both EC and EO within 5 and 15 Hz were included in the next steps of the analysis ( $n = 1,820$ ). The final EEG sample included only subjects where FOOOF models accurately fit the individual power spectrum ( $r^2 > 0.75$ ; final EEG sample size = 1,388). Alpha power, frequency, and bandwidth were estimated for each participant and condition. The relationship

between alpha features and white matter was tested after intersecting the dMRI and EEG samples (final EEG-dMRI sample size  $n = 585$ ; Fig. 1).

*Experimental design and statistical analysis.* Statistical details of each analysis can be found in the corresponding Results subsection.

## Results

### Structural bases of alpha

Individual alpha properties including central frequency, power, and bandwidth corrected for the aperiodic component were estimated with the FOOOF toolbox (Donoghue et al., 2020b). These alpha estimates were calculated separately for EC and EO resting state conditions. DMRI data were processed with QSIprep (Cieslak et al., 2021), and tractometry was performed with pyAFQ (Krupar et al., 2021) and manually quality controlled (Richie-Halford et al., 2022b) to identify the optic radiations (and control pathways) in each individual's brain. We first tested whether alpha features were related to the average FA of the optic radiations by fitting a linear mixed effects (LME) model of FA that included alpha frequency, power, bandwidth, and age as fixed effects. The site location was included as a random effect [for site effects in the HBN dataset see Richie-Halford et al. (2022b)]. Frequency was the only alpha feature that was consistently related to the optic radiations FA across EO/EC conditions (frequency, EC,  $\beta = 0.003$ ,  $SE = 0.001$ ,  $t = 2.65$ ,  $p = 0.008$ ; EO,  $\beta = 0.002$ ,  $SE = 0.001$ ,  $t = 2.58$ ,  $p = 0.01$ ; power, EC,  $\beta = 0.008$ ,  $SE = 0.003$ ,  $t = 2.32$ ,  $p = 0.02$ ; EO,  $\beta = 0.005$ ,  $SE = 0.004$ ,  $t = 1.06$ ,  $p = 0.29$ ; bandwidth, EC,  $\beta = 0.001$ ,  $SE = 0.001$ ,  $t = 0.06$ ,  $p = 0.95$ ; EO,  $\beta = -0.001$ ,  $SE = 0.001$ ,  $t = 0.71$ ,  $p = 0.48$ ), although the effect of alpha power was also observed in EC (as in Tröndle et al., 2022). A separate LME model only focused on alpha frequency showed that an increase of 0.002 in optic radiations FA

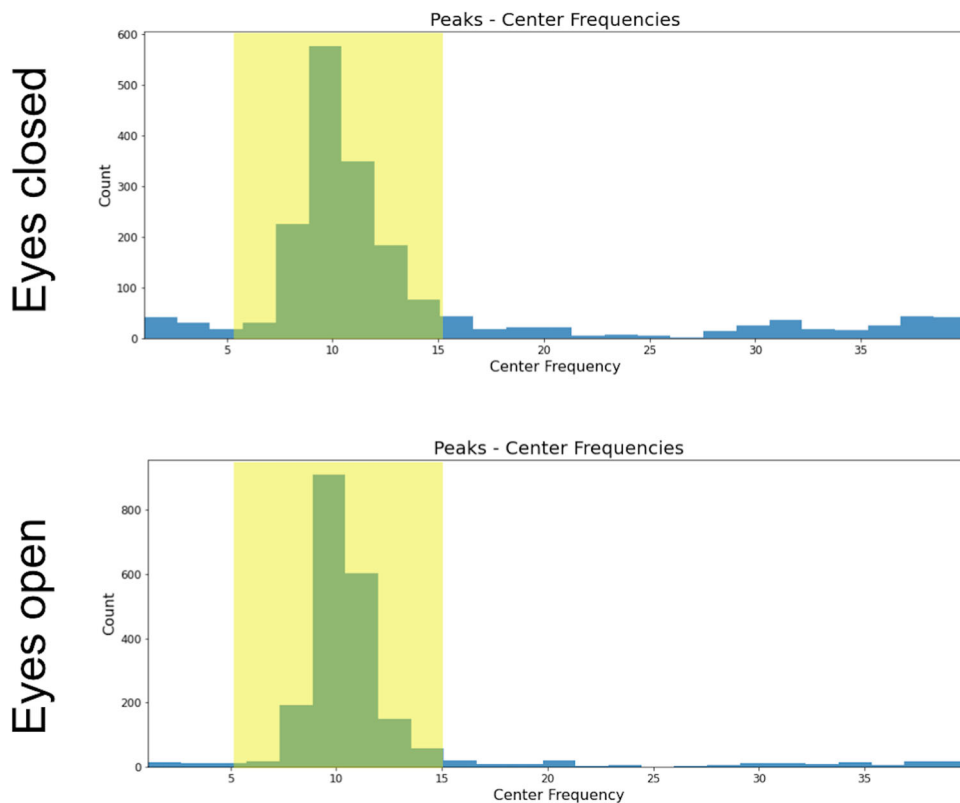


**Figure 2.** Most participants had a maximum peak within alpha frequency range for both EO and EC conditions.

corresponded to an increase of 1 Hz in the alpha frequency after accounting for age and site location (EC:  $\beta = 4.26$ ,  $SE = 1.85$ ,  $t = 2.30$ ,  $p = 0.021$ , EO:  $\beta = 5.20$ ,  $SE = 2.58$ ,  $t = 2.01$ ,  $p = 0.044$ ;

Fig. 3). Adding the factor of optic radiations average length did not improve the model fit (starting model, BIC = 1,836; after adding fiber length BIC = 1,852), suggesting that individual alpha

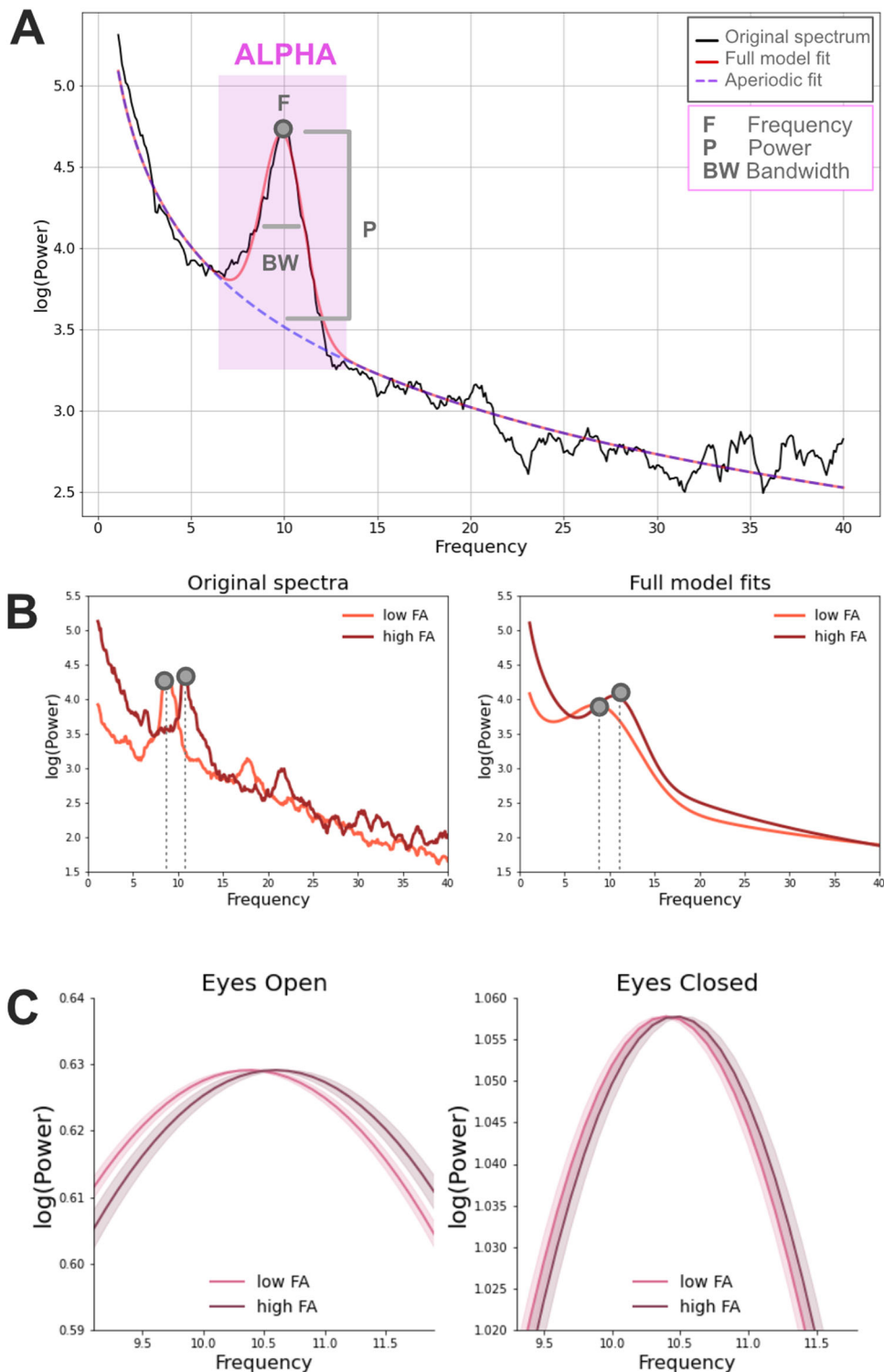


**Figure 3.** *A*, Example of a power spectrum from a 5-year-old male participant (in black) with closed eyes (EC). The corresponding F000F model fit is displayed in red and it corresponds to the sum of the periodic (Gaussian function included in the purple square) and the aperiodic signal (dashed line). Three different estimates are extracted from the periodic signal within the alpha frequency range: power, central frequency, and bandwidth. *B*, Examples of original power spectra and corresponding full F000F model fits (periodic + aperiodic components) in the EC condition. Data come from two representative male participants of 12 years of age with high and low FA average values (high FA = 0.55; low FA = 0.50; median FA = 0.53). *C*, Relationship between alpha frequency (after correcting for the aperiodic component) and the FA of the optic radiations in the EC and EO conditions in the full participant sample. Model fits of the periodic signal are shown for high and low FA participants (defined based on a median split). Beta estimates of alpha frequency were calculated based on the following LME model:  $\alpha \sim FA + \text{age} + (1|s)$ . Model fits of the periodic signal were derived based on the formula  $\text{Gaussian} = \text{power} \cdot e^{-((\text{frequency} - \text{central frequency})^2 / (2 \cdot \text{bandwidth}^2))}$ . The shaded areas represented  $\pm 1$  SE.

frequency could be better predicted based on optic radiations FA than fiber length. These results were confirmed when considering a bigger EEG-dMRI sample ( $n = 783$ ) where the alpha estimates were calculated only based on the EC condition (EC:  $\beta = 3.77$ ,  $SE = 1.71$ ,  $t = 2.20$ ,  $p = 0.03$ ).

We next examined which part of the optic radiation was related to alpha frequency by fitting the same LME models for each node along the tract profile ( $n$  nodes = 100). The LME models included age and alpha as fixed effects and scan site location as a random effect. The alpha-FA relationship was mainly observed in the central and posterior parts of the optic radiations (Fig. 4, panels A,B; for GAM model results, see panels C and D).

We checked for the anatomical specificity of the alpha frequency effect on the optic radiation by running LME models on a set of control tracts. These models tested the relationship between alpha frequency and FA after correcting for age and site location (reference coefficients for optic radiations: EC,  $\beta = 4.26$ ,  $SE = 1.85$ ,  $t = 2.30$ ,  $p = 0.021$ ; EO,  $\beta = 5.20$ ,  $SE = 2.58$ ,  $t = 2.01$ ,  $p = 0.044$ ). We did not see a relationship with alpha frequency in other corticothalamic pathways (anterior thalamic radiation: EC,  $\beta = 1.24$ ,  $SE = 1.75$ ,  $t = 0.71$ ,  $p = 0.48$ ; EO,  $\beta = 1.68$ ,  $SE = 2.36$ ,  $t = 0.72$ ,  $p = 0.47$ ) or in other white matter pathways that end in the posterior part of the cortex (occipital segment of the corpus callosum: EC,  $\beta = 0.26$ ,  $SE = 1.37$ ,  $t = 0.19$ ,  $p = 0.85$ ; EO,  $\beta = 3.33$ ,  $SE = 2.05$ ,  $t = 1.63$ ,  $p = 0.10$ ; posterior parietal segment of the corpus callosum: EC,  $\beta = 0.93$ ,  $SE = 1.31$ ,  $t = 0.71$ ,  $p = 0.48$ ; EO,  $\beta = 0.32$ ,  $SE = 1.61$ ,  $t = 0.20$ ,  $p = 0.85$ ; inferior fronto-occipital fasciculus: EC,  $\beta = 0.89$ ,  $SE = 2.17$ ,  $t = 0.41$ ,  $p = 0.68$ ; EO,  $\beta = 1.77$ ,  $SE = 3.00$ ,  $t = 0.59$ ,  $p = 0.56$ ; Fig. 5).

### Other white matter microstructural properties

FA of the optic radiations was our primary focus as it represents the diffusion property that has been most largely reported to correlate with electrophysiological measures (Dubois et al., 2008; Westlye et al., 2009; Whitford et al., 2011; Kemmotsu et al., 2012; Taddei et al., 2012; Lobsien et al., 2014; Price et al., 2017; Gao et al., 2017b; Shin et al., 2019; Takemura et al., 2020). Additional microstructural properties of the optic radiation were explored to better understand the nature of the alpha-white matter link. While alpha frequency was not related to MD (EC,  $\beta = -2.12$ ,  $SE = 1.76$ ,  $t = 1.21$ ,  $p = 0.23$ ; EO,  $\beta = -0.67$ ,  $SE = 1.14$ ,  $t = 0.58$ ,  $p = 0.56$ ), there was a relationship with the axonal water fraction (AWF) calculated with the “white matter tract integrity model” as implemented in DIPY (Fieremans et al., 2011; Garyfallidis et al., 2014; Henriques et al., 2021; EC,  $\beta = 6.54$ ,  $SE = 2.74$ ,  $t = 2.39$ ,  $p = 0.02$ ; EO,  $\beta = 6.88$ ,  $SE = 3.96$ ,  $t = 1.74$ ,  $p = 0.08$ ). In the EC condition, every increase of 1 Hz in the alpha frequency corresponded to an increase of 0.001 in optic radiations AWF after accounting for age and site location.

### Developmental changes in alpha and optic radiations

A clear developmental trajectory could be observed in the EEG periodic and aperiodic signals (Figs. 6, 7), as well as in the optic radiations FA (Fig. 8). Between 5 and 21 years of age, alpha frequency, power, and bandwidth increased after correcting for the aperiodic component (as in Tröndle et al., 2022; frequency, EC,  $r = +0.36$ ,  $p = 2 \times 10^{-19}$ ; EO,  $r = +0.34$ ,  $p = 1 \times 10^{-17}$ ; power, EC,  $r = +0.18$ ,  $p = 2 \times 10^{-5}$ ; EO,  $r = +0.05$ ,  $p = 0.26$ ; bandwidth, EC,  $r = +0.17$ ,  $p = 4 \times 10^{-5}$ ; EO,  $r = +0.12$ ,  $p = 0.004$ ; Figs. 6, 7). Moreover, the optic radiations FA increased with age ( $r = +0.30$ ,  $p = 9 \times 10^{-12}$ ).

Despite these robust developmental changes, the alpha-optic radiation relationship was consistent across development. For

instance, adding the interaction between age and optic radiations FA [ $\alpha \sim \text{FA} * \text{age} + (1|\text{siteID})$ ] did not improve the fit of the LME model (BIC = 1,836; after adding the interaction BIC = 1,839), which suggests that the alpha-white matter link was present even after controlling for additive and interactive developmental effects.

We further tested whether developmental changes in the optic radiation mediate the development of alpha by performing a causal mediation analysis (Tingley et al., 2014). Two linear regression models were specified: a mediator model estimating the effect of age on FA and an outcome model estimating the effect of age and FA on alpha frequency for both EC and EO. The mediation R package (Tingley et al., 2014) uses these two models as starting points to compute the average “causal mediation effect” (indirect effect of age on alpha that is related to the FA mediator) and the average direct effect (effect of age on alpha after partialling out the FA mediator effect). The sum of these two effects resulted in the total effect of age on alpha. A bootstrap analysis with 1,000 simulations was used to calculate the uncertainty estimates of these effects (Efron and Tibshirani, 1994). This analysis showed that the development of the optic radiation partially mediated developmental changes of alpha frequency [EC, average causal mediation effect,  $\beta = 0.008$ , CI (0.009; 0.02),  $p = 0.034$ ; percentage of age effect that is due to the FA mediator, 6.44%,  $p = 0.034$ ; EO, average causal mediation effect,  $\beta = 0.011$ , CI (0.002; 0.02),  $p = 0.02$ ; percentage of age effect that is due to the FA mediator, 6.77%,  $p = 0.02$ ; Fig. 9]. The effect of age on alpha was still present after taking into account the mediator [EC, average direct effect,  $\beta = 0.11$ , CI (0.09; 0.14),  $p < 0.001$ ; EO, average direct effect,  $\beta = 0.15$ , CI (0.12; 0.18),  $p < 0.001$ ], suggesting that FA variations partially mediated alpha development. A mediation model where alpha was considered a mediator, instead of FA, led to similar results but lower percentages of age effect explained by the mediator (EC, 1.15%; EO, 1.09%). A similar mediation effect was observed with optic radiations AWF for the EC condition [EC, average causal mediation effect,  $\beta = 0.014$ , CI (0.003; 0.03),  $p = 0.022$ ; percentage of age effect that is due to the AWF mediator, 11.57%,  $p = 0.022$ ; EO, average causal mediation effect,  $\beta = 0.015$ , CI (-0.0001; 0.03),  $p = 0.054$ ; percentage of age effect that is due to the AWF mediator, 9.22%,  $p = 0.054$ ]. None of the control tracts examined above showed a mediation effect of FA on the maturational trajectories of alpha frequency [average causal mediation effects in anterior thalamic radiation: EC,  $\beta = 0.0027$ , CI (-0.008; 0.012),  $p = 0.59$ ; EO,  $\beta = 0.005$ , CI (-0.007; 0.018),  $p = 0.40$ ; occipital segment of the corpus callosum: EC,  $\beta = 0.0007$ , CI (-0.007; 0.008),  $p = 0.88$ ; EO,  $\beta = 0.01$ , CI (-0.002; 0.023),  $p = 0.09$ ; posterior parietal segment of the corpus callosum: EC,  $\beta = 0.0018$ , CI (-0.004; 0.007),  $p = 0.56$ ; EO,  $\beta = 0.0007$ , CI (-0.009; 0.009),  $p = 0.88$ ; inferior fronto-occipital fasciculus: EC,  $\beta = 0.0016$ , CI (-0.008; 0.013),  $p = 0.73$ ; EO,  $\beta = 0.005$ , CI (-0.009; 0.019),  $p = 0.47$ ].

### Behavioral correlates of alpha

Finally, we explored behavioral correlates of occipital alpha by extracting measures of visual perception for each individual. Participants performed a visual contrast change detection task where they were presented with an annular pattern ( $1^\circ$  of inner radius;  $6^\circ$  of outer radius), which consisted of two overlaid gratings (each one tilted  $45^\circ$  to the left and right, respectively). At the beginning of the trial, these two gratings had the same visual image contrast (50%). Within the following 1,600 ms, one of the two gratings gradually changed its contrast to 0% while the

## Optic Radiation

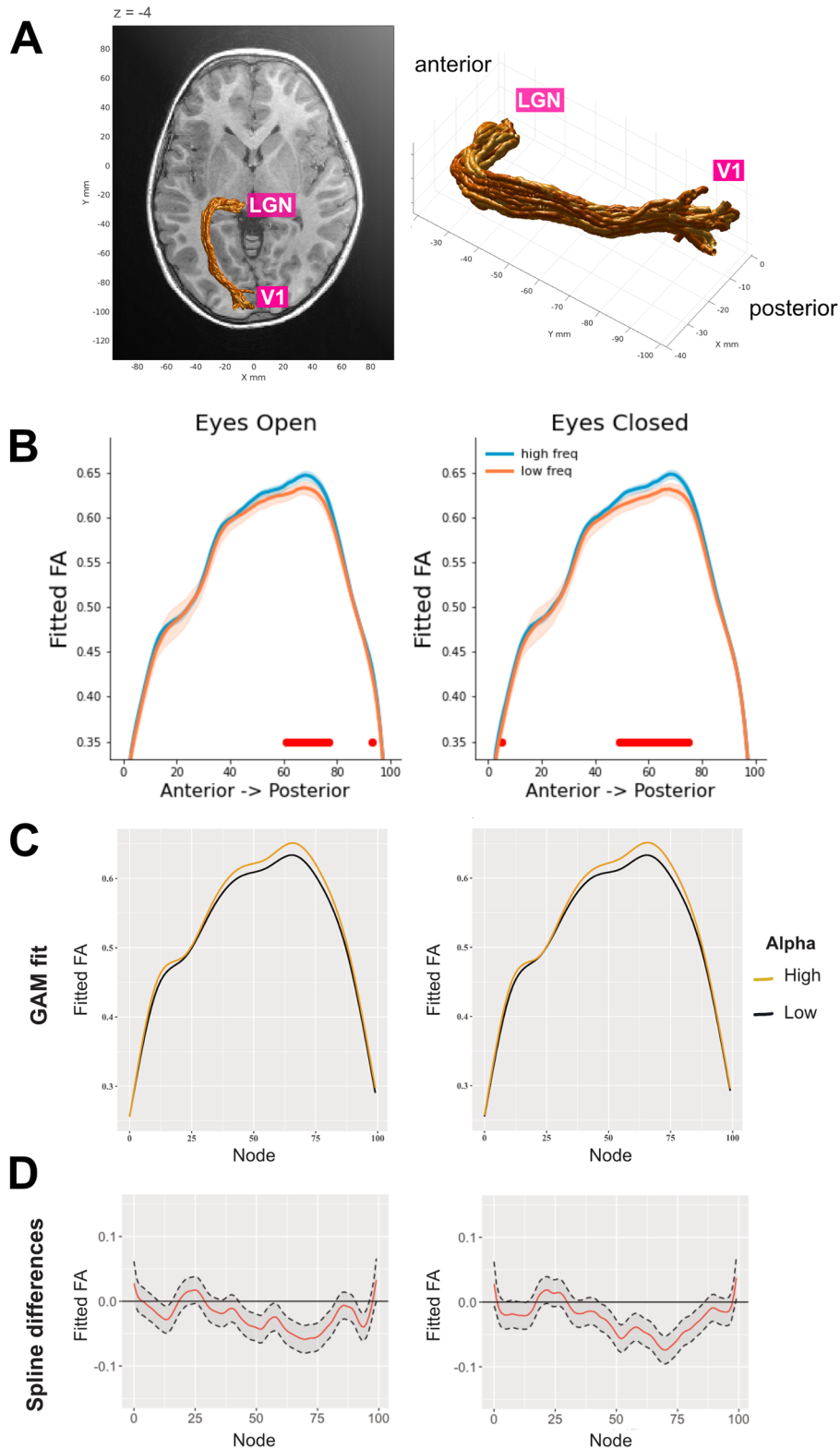


**Figure 4.** *A*, Three-dimensional rendering of the left optic radiation for a single representative participant (5-year-old female). The rendering was derived from the Automated Fiber Quantification software (Yeatman et al., 2012). *B*, Tract profiles of the optic radiations FA for each alpha frequency group (defined based on a median split) in EC and EO conditions. The plots show FA values estimated based on the beta coefficients extracted from node-by-node LME models. The optic radiations FA was modeled as a function of alpha frequency after accounting for age and site location [i.e.,  $FA \sim \alpha \text{ frequency} + \text{age} + (1|\text{site})$ ]. The red horizontal lines highlight the nodes where FDR-corrected  $p$ -values are below 0.025. The shaded areas represent  $\pm 1$  SE. *C, D*, GAM results for tract profile analyses. We adopted a multi-analysis approach where both LME and GAM models were applied for tract profile analyses [following the guidelines from Wagenmakers et al. (2022)]. GAM models were run on the dMRI-EEG sample ( $n = 585$ ) using the tractable R package (<https://github.com/yeatmanlab/tractable>; Richie-Halford et al., 2023, which implements the pipeline reported in Muncy et al., 2022). Our GAM formula was  $FA \sim \text{age} + \alpha \text{ frequency} + s(\text{nodeID}, \text{by} = \alpha \text{ frequency}, k = 64) + s(\text{subjectID}, \text{bs} = "re")$ . *C*, Similar to what was seen in the results from the node-by-node LME models, GAM model fits showed that alpha frequency had an impact on the optic radiations FA, and this effect was mainly localized in the centro-posterior part of the tract (EO, estimate = 0.021, SE = 0.002,  $t = 12.03$ ; EC, estimate = 0.024, SE = 0.002,  $t = 13.73$ ). *D*, Spline differences are shown with a 95% confidence interval.

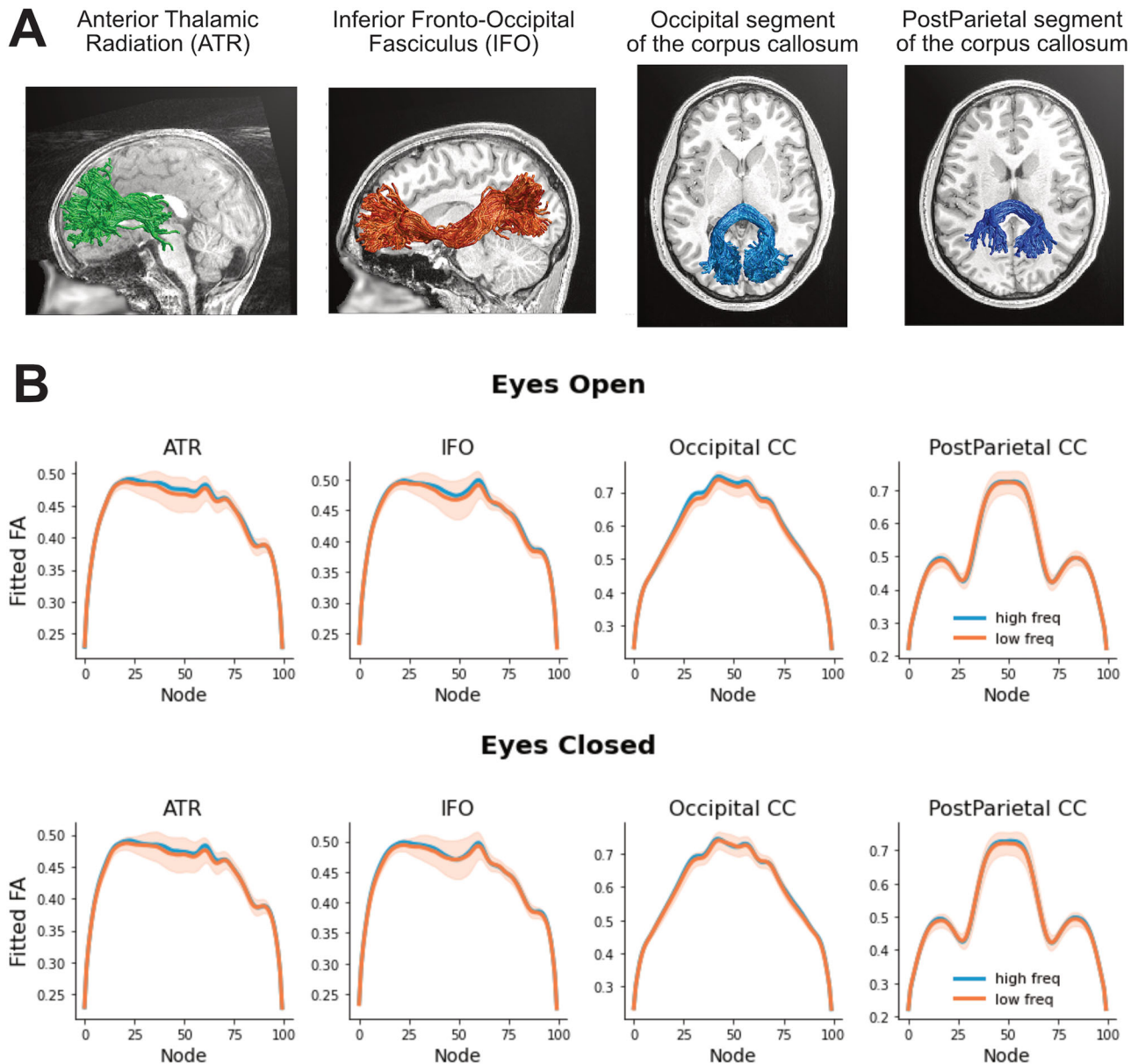


**Figure 5.** *A*, Three-dimensional rendering of the control tracts from three representative participants (ATR, 6-year-old male; post-parietal, 7-year-old female; IFO and occipital, 12-year-old male). *B*, Tract profiles of control tracts for each alpha frequency group (defined based on a median split) in EC and EO conditions (first and second rows, respectively). The plots show FA values estimated based on the beta coefficients extracted from node-by-node LME models. The shaded areas represent  $\pm 1$  SE.

other reached a contrast of 100% [total of three blocks with 24 trials each, equally distributed across left and right sides; the experimental paradigm is described in detail by Langer et al., (2017)]. Participants were asked to press one of two response buttons based on the grating that had the strongest contrast. After 800 ms, the gratings' contrast level came back to baseline (50%), and participants received feedback on their trial performance (ITI could be 2.8, 4.4, or 6 s). Individual average accuracy scores were calculated, and only participants with above-chance performance were considered ( $n = 917$ ; average accuracy, 83.66; SD, 0.12). A linear regression model was fitted to these accuracy measures including alpha features (power, frequency, bandwidth) and age as factors. Individual alpha frequency was the only electrophysiological property related to contrast detection accuracy (EC,  $\beta = 0.011$ ,  $SE = 0.003$ ,  $t = 3.34$ ,  $p < 0.001$ ,  $R^2 = 27.7\%$ ; EO,  $\beta = 0.008$ ,  $SE = 0.003$ ,  $t = 3.18$ ,  $p = 0.002$ ,  $R^2 = 27.5\%$ ). Drift

diffusion models (Wiecki et al., 2013) were also run in order to combine reaction times and accuracy scores within the same dependent variable. Individual drift rates were obtained, which correspond to an estimate of the rate at which the visual system extracts information to inform a decision. The drift rate was associated with alpha frequency (EC,  $\beta = 0.072$ ,  $SE = 0.030$ ,  $t = 2.42$ ,  $p = 0.016$ ,  $R^2 = 13.8\%$ ; EO,  $\beta = 0.064$ ,  $SE = 0.023$ ,  $t = 2.70$ ,  $p = 0.007$ ,  $R^2 = 13.7\%$ ), suggesting that participants with a fast alpha rhythm also extracted visual information more efficiently than participants with a slow alpha rhythm (i.e., they had a high drift rate on the visual detection task). Moreover, mediation analysis showed that developmental changes of accuracy scores were mediated by alpha frequency changes [EC, average causal mediation effect:  $\beta = 0.002$ , CI (0.001; 0.002),  $p < 0.001$ ; percentage of age effect that is due to the alpha mediator: 8.08%,  $p < 0.001$ ; EO, average causal mediation effect:  $\beta = 0.001$ , CI (0.001;

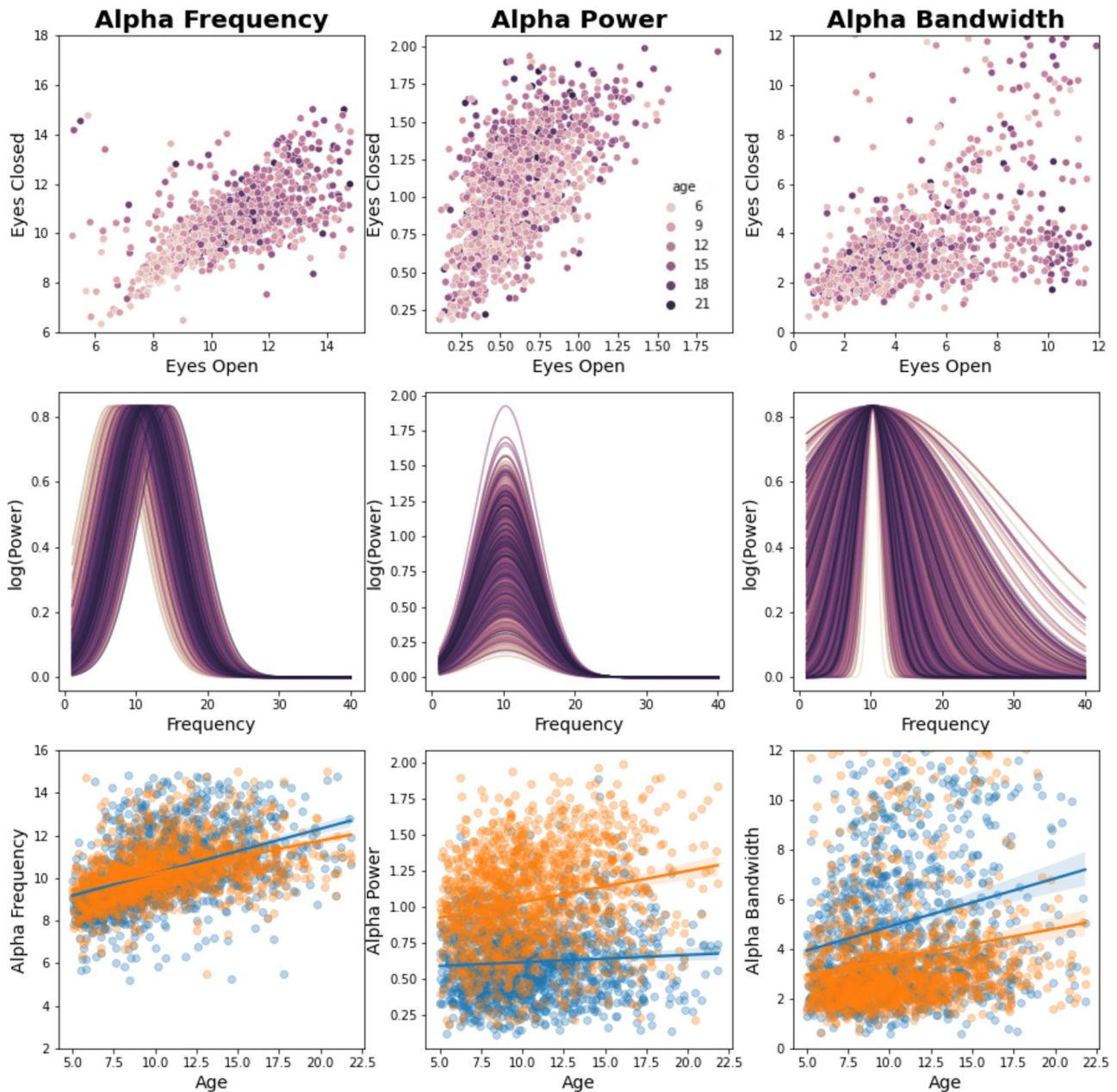


**Figure 6.** Developmental effects on EC and EO alpha (F000F periodic signal). Individual alpha properties (frequency, power, and bandwidth) are shown for each condition (EC and EO). The first row shows that alpha frequency and power in EC highly correlate with alpha frequency and power in EO, suggesting that a similar electrophysiological phenomenon is observed across conditions. The second row shows the effect of age on individual F000F (Donoghue et al., 2020b) models of alpha [calculated as Gaussian =  $\text{Power} * e^{-((\text{frequency} - \text{central frequency})^2 / (2 * \text{bandwidth}^2))}$ ], where alpha measures from EC and EO conditions were averaged]. The third row shows the relationships between alpha features and age for both EC (orange) and EO (blue) conditions.

0.002),  $p < 0.001$ ; percentage of age effect that is due to the alpha mediator: 7.39%,  $p < 0.001$ ; Fig. 9]. Similar mediation effects of alpha were observed with developmental changes of drift rate scores, although only in the EC condition (EC, average causal mediation effect:  $\beta = 0.007$ , CI (0.0003; 0.01),  $p = 0.046$ ; percentage of age effect that is due to the alpha mediator: 9.24%,  $p = 0.046$ ; EO, average causal mediation effect:  $\beta = 0.006$ , CI (-0.002; 0.01),  $p = 0.13$ ). To test for the specificity of alpha behavioral correlates, we ran a follow-up analysis exploring the relationship between alpha features and a control task focused on sequence learning. Participants were required to memorize and reproduce a sequence of circle positions (six or eight circle positions, depending on the participants' age). The sequence was

repeated five times, and participants provided their responses at the end of each repetition (average accuracy, 48%; SD, 23). Similarly to the analysis on the visual detection task, a linear regression model was fitted to the sequence learning accuracy scores (i.e., mean accuracy over the five repetitions) including alpha features (power, frequency, bandwidth) and age as factors. Alpha frequency was not related to sequence learning accuracy, and the percentage of variance explained by the alpha models dropped from about 27% for visual detection to 4% for sequence learning (EC,  $\beta = 0.005$ ,  $SE = 0.007$ ,  $t = 0.70$ ,  $p = 0.482$ ,  $R^2 = 3.6\%$ ; EO,  $\beta = 0.002$ ,  $SE = 0.006$ ,  $t = 0.40$ ,  $p = 0.692$ ,  $R^2 = 4.3\%$ ). This points to a specific relationship between alpha frequency and visual detection performance.



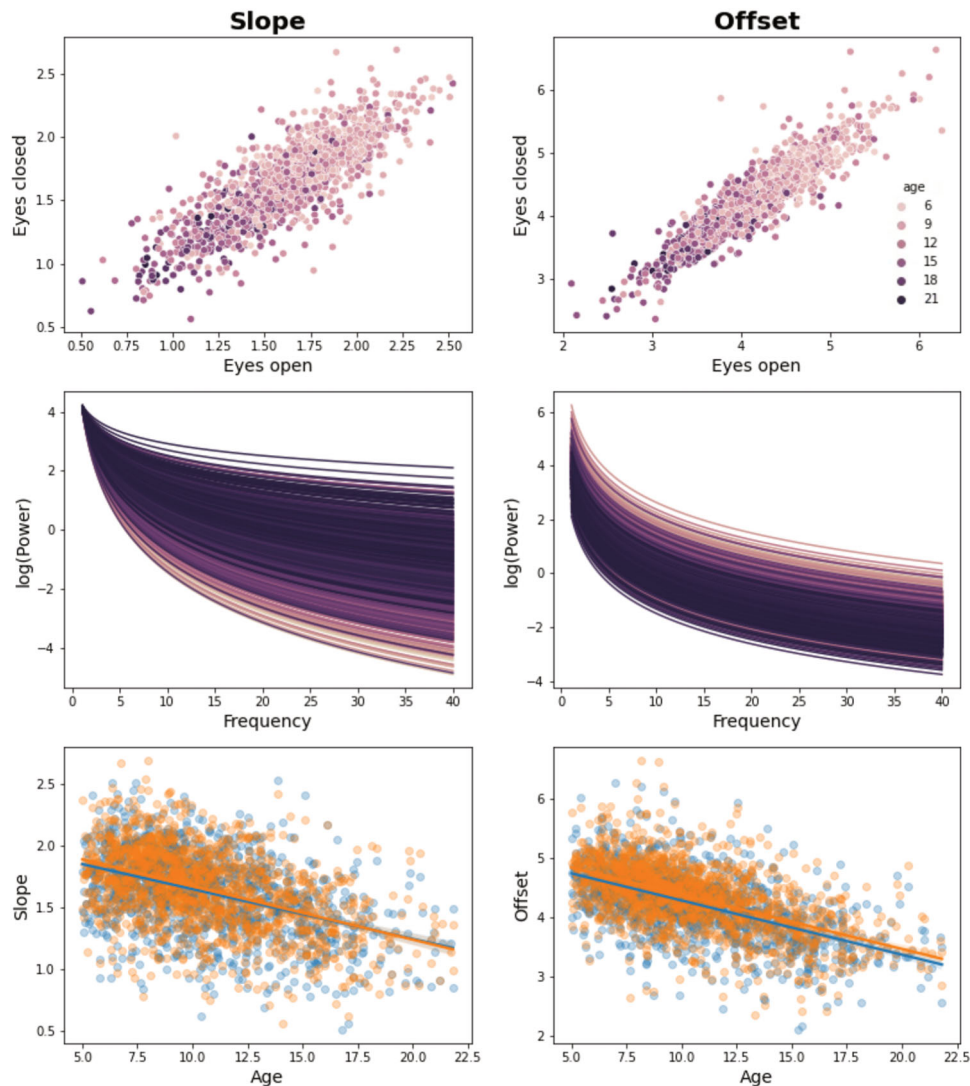


**Figure 7.** Developmental effects on EEG signal (FOOF aperiodic signal). Individual properties of the EEG aperiodic signal (slope and offset) are shown. The first row shows that EEG slope and offset in EC highly correlate with EEG slope and offset in EO, suggesting that a similar electrophysiological phenomenon is observed across conditions. The second row shows the effect of age on individual FOOF (Donoghue et al., 2020b) models of EEG aperiodic signal [calculated as  $\log(\text{power}) = \text{offset} - \log(\text{frequency}^{\text{slope}})$ , where slope and offset measures from EC and EO conditions were averaged]. The third row shows the relationships between alpha features and age for both EC (orange) and EO (blue) conditions. As already reported in previous studies (Donoghue et al., 2020a; Cellier et al., 2021; Tröndle et al., 2022), during development the EEG aperiodic slope becomes flatter, and its offset reduces (hence, the overall power of EEG signal decreases). Changes in slope and offset have been related to general developmental changes involving the skull and/or the brain. It has been proposed that age-related slope changes are due to variations in the ratio between neural inhibition and excitation or increased asynchronous neural activity (Gao et al., 2017a). On the other hand, the offset reduction has been related to the increasing resistance of the skull (which becomes thicker with age), the decreasing overall spiking activity due to synaptic pruning, or the co-occurrent flattening of the slope (Tröndle et al., 2022). An LME model testing whether overall FA scores of individual subjects (i.e., average FA values of all default pyAFQ bundles) are related to aperiodic signal properties showed an effect of the offset, but not of the slope, after accounting for age and site location (offset,  $\beta = -0.005$ ,  $SE = 0.002$ ,  $t = 2.33$ ,  $p = 0.02$ ; slope,  $\beta = 0.003$ ,  $SE = 0.004$ ,  $t = 0.97$ ,  $p = 0.33$ ). This seems to suggest that offset changes are not exclusively related to skull/slope changes, but can reflect widespread variations in white matter fiber structure and possibly pruning.

We finally tested whether the optic radiations FA further contributed to explaining the variability in visual perception performances by examining a sample of participants that have EEG, dMRI, and behavioral measures available ( $n = 399$ ). A linear regression model on this smaller dataset confirmed the effect of EC alpha frequency on visual accuracy (EC,  $\beta = 0.012$ ,  $SE = 0.006$ ,  $t = 2.04$ ,  $p = 0.042$ ,  $R^2 = 26.5\%$ ; EO,  $\beta = 0.005$ ,  $SE = 0.004$ ,  $t = 1.46$ ,  $p = 0.15$ ,  $R^2 = 26.4\%$ ). However, no effect on visual accuracy could be observed for the optic radiations FA (EC,  $\beta = 0.13$ ,  $SE = 0.19$ ,  $t = 0.71$ ,  $p = 0.48$ ; EO,  $\beta = 0.13$ ,  $SE = 0.19$ ,  $t = 0.70$ ,  $p = 0.49$ ) or AWF (EC,  $\beta = 0.05$ ,  $SE = 0.03$ ,  $t = 0.15$ ,  $p = 0.88$ ; EO,  $\beta = 0.09$ ,  $SE = 0.30$ ,  $t = 0.30$ ,  $p = 0.76$ ). No significant effects were observed in the drift rate analysis for this sample.

## Discussion

This work capitalized on a large dMRI-EEG developmental sample and uncovered the relationship between the structure of visual white matter pathways, properties of spontaneous alpha rhythm, and behavior. It showed for the first time specific mediation effects between the maturation of optic radiation, development of spontaneous electrophysiological activity, and maturational trajectories of human vision.

Our results showed that alpha frequency at rest is specifically related to the FA of optic radiations: children and adolescents with a fast alpha rhythm tend to show high FA values of the optic radiations. This structural–functional relationship was observed after accounting for age effects, suggesting that alpha oscillations

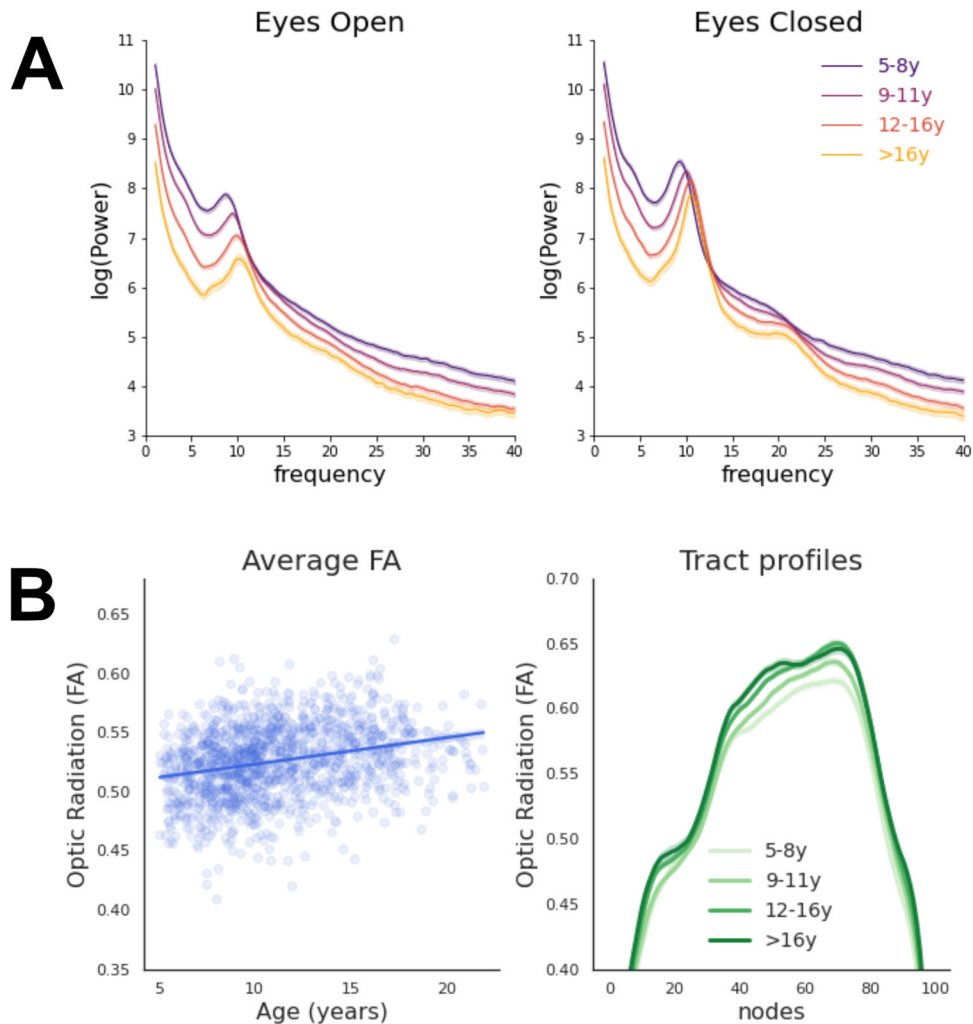


**Figure 8.** *A*, Developmental trajectory of the power spectra in the EEG final sample ( $n = 1,388$ ) for EC and EO conditions. Age groups approximately correspond to different developmental stages: pre-puberty (5–8 years,  $n = 373$ ), early adolescence (9–11 years,  $n = 488$ ), mid-adolescence (12–16 years,  $n = 416$ ), and late adolescence (>16 years,  $n = 111$ ; Salmela-Aro, 2011). Developmental trajectories of the periodic and aperiodic signals calculated with F000F are displayed separately in Figures 6 and 7. *B*, Developmental trajectory of the optic radiations FA values in the dMRI final sample ( $n = 1,394$ ). Average FA values and FA values along the tract profile are displayed on the left and right panels, respectively. Age groups correspond to pre-puberty (5–8 years,  $n = 308$ ), early adolescence (9–11 years,  $n = 481$ ), mid-adolescence (12–16 years,  $n = 436$ ), and late adolescence (>16 years,  $n = 180$ ; Salmela-Aro, 2011). All shaded areas represent  $\pm 1$  SE.

have a consistent structural correlation between 5 and 21 years old, which does not seem to vary across age groups. Note that this effect is relatively small (about 6% of age-related alpha variations were explained by the developmental changes of FA), which might explain the difficulty of detecting this effect in smaller samples (Renauld et al., 2016). Among the optic radiation structural properties that can be at the basis of alpha frequency variations are axonal density, axonal size, fiber spatial organization, myelination, and glial cell structural properties (which can all affect FA values, Jeurissen et al., 2013; De Santis et al., 2014; Jeurissen et al., 2013; De Santis et al., 2014), while fiber length does not seem to play a crucial role. Our follow-up analyses on additional white matter properties helped to clarify the nature of the observed white matter-alpha link. The analyses of optic radiations AWF, a measure that is sensitive to myelin volume, number of axons, and axonal geometry (Fieremans et al., 2011), showed that participants with higher AWF levels also had faster alpha rhythm. This suggests that optic radiation axonal size, density, or myelination might be linked to alpha frequency. In addition, the fact that alpha was related to FA but not MD measures (see Valdés-Hernández et al., 2010; Lobsien et al.,

2014 for a similar asymmetry) suggests that fiber orientation coherence is another potential factor related to alpha. For instance, fiber orientation coherence is likely to affect FA more than MD (Uddin et al., 2019; Luque Laguna et al., 2020), and it also has an impact on neural synchronization, which ultimately modulates the EEG activity measured on the scalp (da Silva, 2010; Bressler, 2011). Overall, the observed link between visual white matter microstructural properties and occipital electrophysiological responses supports the idea that the optic radiations axonal density, myelination, and/or spatial coherence contribute to the degree of synchrony with which white matter fibers deliver neural signals to the cortex, which are finally reflected by oscillatory brain activity measured on the scalp (Dubois et al., 2008; Hindriks et al., 2015; Minami et al., 2020; Takemura et al., 2020). Future work can further explore and clarify the directionality of the link between specific white matter properties and functional connectivity between cortical and sub-cortical alpha sources. It is also feasible that developmental changes in alpha could induce changes in white matter properties. Considering causality requires experimental manipulations that are beyond the scope of this work.

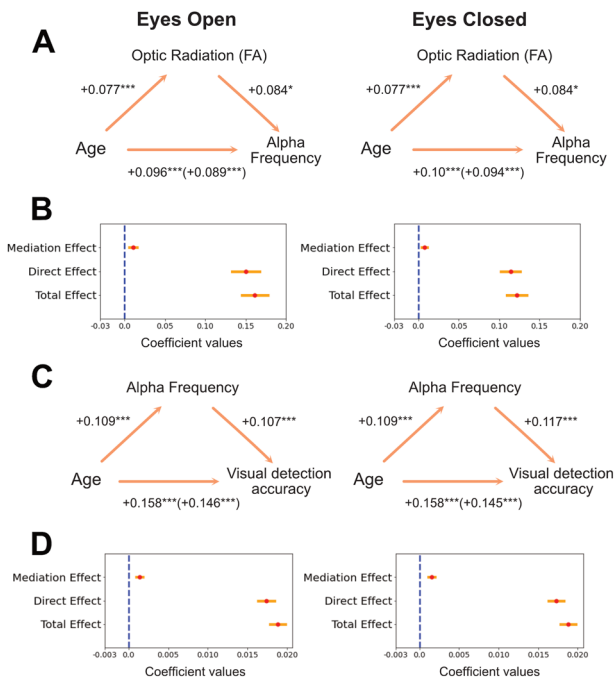


**Figure 9.** *A*, Mediation effect of the optic radiations FA on alpha development. Schematic representation of the mediation analysis results. Standardized coefficients are reported. *B*, Beta coefficients of the main effects of the mediation analysis represented in *A* are displayed in red. Yellow bars represent  $\pm 1$ SE. *C*, Schematic representation of the mediation analysis of alpha on visual detection development. Standardized coefficients are reported. *D*, Beta coefficients of the main effects of the mediation analysis of alpha on visual detection development (represented in *C*).

The generalization of the structural basis of alpha across species also remains unclear and needs further investigation. While there is some evidence of the behavioral and functional significance of alpha in other primates (Haegens et al., 2011; Mo et al., 2011; Jensen and Bonnefond, 2013), the link between alpha and white matter has not been reported in macaque monkeys so far (whose visual system represents one of the closest approximations of the human's one). This potential difference between humans and primates might be due to the reduced amount of research on the alpha–FA link in primates, technical divergences across studies, or evolutionary differences between species (e.g., the visual cortex is about 55% of the occipital lobe in macaques while 30% in humans; Tootell et al., 2003).

The portions of white matter fibers that were mainly related to alpha frequency were located in the central and posterior segments of the optic radiations. There are at least two possible explanations for the location of this effect. First, this segment of the tract represents the closest location to the alpha recording site and cortical generators. Second, the posterior part of the optic radiation has a higher signal-to-noise ratio (and smaller SE) as compared to the anterior segment, which is probably due to the large size of the posterior endpoint ROI (V1) and a more linear trajectory of the posterior as compared to the anterior segment of the tract (Sherbondy et al., 2008). Paying special attention to the definition of the anterior ROIs used in optic radiation tractometry can improve the precision and reliability of automated white matter segmentation, which is crucial when working with large samples (Kruper et al., 2021).

Our findings also showed that development of the optic radiations specifically accounts for changes in alpha frequency between childhood and late adolescence. Between 5 and 21 years of age

visual networks undergo a large range of structural and functional transformations. Visual white matter pathways increase their structural coherence, axonal diameter, axonal density, and myelination (Tau and Peterson, 2010; Chang et al., 2015; Lynch et al., 2020). This happens with a concomitant increase of FA and AWF values and improved signal transmission (Barnea-Goraly et al., 2005). At the same time, the rhythm of spontaneous occipital alpha speeds up (Cellier et al., 2021), which probably reflects a higher precision in neural synchrony over long distances and greater coherence between thalamocortical alpha generators (Uhlhaas et al., 2010). Our findings showed for the first time that these two maturational phenomena are interrelated, with structural changes of the optic radiations (FA and AWF) mediating the development of alpha oscillations between 5 and 21 years of age. This result further complements previous reports showing a link between the development of the optic radiations and other types of electrophysiological responses, such as early visual evoked responses peaking around 100 ms (Caffarra et al., 2021). Overall, these findings suggest that the maturation of the optic radiations (and possibly a greater myelination/fiber spatial orientation coherence) accounts for changes in the precision and frequency of neural synchronization within the alpha band (i.e., rhythmic neural activity every 100 ms). Future longitudinal studies will help clarify the temporal sequence of these structural and functional changes during development.

Finally, this is the first study to create a bridge within the same dataset between the development of optic radiation, alpha frequency, and visual perception. Our visual detection task analyses highlighted that the development of spontaneous alpha activity has specific implications for visual perception. Data from behavioral tasks confirmed that the individual variability observed in alpha frequency is linked to changes in the efficiency of visual perception, but not to sequence learning performance. Participants with a fast alpha rhythm showed a more accurate performance at an image contrast detection task and a higher rate of visual information extraction. One possible explanation of this phenomenon is that people with fast alpha sample visual information at higher rates (Samaha and Postle, 2015), resulting in more evidence accumulation to inform the detection decision and higher cognitive capacities (as more information can be extracted in a short amount of time, Di Gregorio et al., 2022). These results are in line with previous reports showing that alpha speed determines the temporal resolution at which visual information can be consciously sampled (Samaha and Postle, 2015), as well as studies showing a link between pre-stimulus alpha and conscious visual detection (Ergenoglu et al., 2004; Van Dijk et al., 2008; Mathewson et al., 2009; Lange et al., 2013). All these findings are compatible with the hypothesis that alpha oscillations represent a general electrophysiological mechanism of rhythmic inhibition pulses (every  $\sim 100$  ms) that can cyclically modulate the level of excitability of a given brain area (Jensen and Mazaheri, 2010; Van Diepen et al., 2019; e.g., visual cortex). According to this perspective, spontaneous occipital alpha reflects a general gating mechanism that regulates neural information flow between the thalamus and the visual cortex and ultimately impacts our conscious visual perception. Our findings showed that the maturation of the optic radiation mediates the development of this inhibition mechanism reflected by alpha, which specifically contributes to visual detection accuracy improvement during childhood and adolescence.

In summary, alpha is a predominant rhythm of our brain and its characteristics can widely vary over development. Individual variability in alpha frequency is specifically related to the

structural properties of visual white matter pathways and can ultimately predict the rate of our visual information extraction. This work shows that the maturation of optic radiations is linked to an increase in alpha frequency, which specifically contributes to visual detection enhancement over childhood and adolescence.

## References

- Alexander LM, Escalera J, Ai L, Andreotti C, Febre K, Mangone A, Vega-Potler N, Langer N, Alexander A, Kovacs M (2017) An open resource for transdiagnostic research in pediatric mental health and learning disorders. *Sci Data* 4:170181.
- Altis S (1996) Spectral analysis for physical applications—multitaper and conventional univariate techniques by: D B. Percival and A. T. Walden. *Environ Eng Geosci* II:135.
- Avants BB, Epstein CL, Grossman M, Gee JC (2008) Symmetric diffeomorphic image registration with cross-correlation: evaluating automated labeling of elderly and neurodegenerative brain. *Med Image Anal* 12:26–41.
- Barnea-Goraly N, Menon V, Eckert M, Tamm L, Bammmer R, Karchemskiy A, Dant CC, Reiss AL (2005) White matter development during childhood and adolescence: a cross-sectional diffusion tensor imaging study. *Cereb Cortex* 15:1848–1854.
- Berger H (1938) Über das elektroencephalogramm des menschen. XIV. *Arch Psychiat Nervenkr* 108:407–431.
- Bressler SL (2011) Event-related potentials of the cerebral cortex. In: *Electrophysiological recording techniques* (Vertes RP, Stackman RW Jr, eds), pp 169–190. Totowa, NJ: Humana Press.
- Caffarra S, Joo SJ, Bloom D, Kruper J, Rokem A, Yeatman JD (2021) Development of the visual white matter pathways mediates development of electrophysiological responses in visual cortex. *Hum Brain Mapp* 42:5785–5797.
- Cellier D, Riddle J, Petersen I, Hwang K (2021) The development of theta and alpha neural oscillations from ages 3 to 24 years. *Dev Cogn Neurosci* 50:100969.
- Chang YS, et al. (2015) White matter changes of neurite density and fiber orientation dispersion during human brain maturation. *PLoS One* 10:e0123656.
- Cieslak M, et al. (2021) QSIPrep: an integrative platform for preprocessing and reconstructing diffusion MRI data. *Nat Methods* 18:775–778.
- da Silva FL (2010) EEG: origin and measurement. In: *EEG-fMRI: physiological basis, technique, and applications* (Mulert C, Lemieux L, eds), pp 19–38. Berlin, Heidelberg: Springer Berlin Heidelberg.
- De Santis S, Drakesmith M, Bells S, Assaf Y, Jones DK (2014) Why diffusion tensor MRI does well only some of the time: variance and covariance of white matter tissue microstructure attributes in the living human brain. *Neuroimage* 89:35–44.
- Di Gregorio F, Trajkovic J, Roperti C, Marcantoni E, Di Luzio P, Avenanti A, Thut G, Romei V (2022) Tuning alpha rhythms to shape conscious visual perception. *Curr Biol* 32:988–998.e6.
- Donoghue T, et al. (2020b) Parameterizing neural power spectra into periodic and aperiodic components. *Nat Neurosci* 23:1655–1665.
- Donoghue T, Dominguez J, Voytek B (2020a) Electrophysiological frequency band ratio measures conflate periodic and aperiodic neural activity. *eNeuro* 7:1–14.
- Dubois J, Dehaene-Lambertz G, Soarès C, Cointepas Y, Le Bihan D, Hertz-Pannier L (2008) Microstructural correlates of infant functional development: example of the visual pathways. *J Neurosci* 28:1943–1948.
- Efron B, Tibshirani RJ (1994) *An Introduction to the bootstrap*. New York: CRC Press.
- Ergenoglu T, Demiralp T, Bayraktaroglu Z, Ergen M, Beydagi H, Uresin Y (2004) Alpha rhythm of the EEG modulates visual detection performance in humans. *Brain Res Cogn Brain Res* 20:376–383.
- Fan L, et al. (2016) The human brainnetome atlas: a new brain atlas based on connective architecture. *Cereb Cortex* 26:3508–3526.
- Fieremans E, Jensen JH, Helpert JA (2011) White matter characterization with diffusional kurtosis imaging. *Neuroimage* 58:177–188.
- Gao S, Liu P, Guo J, Zhu Y, Liu P, Sun J, Yang X, Qin W (2017b) White matter microstructure within the superior longitudinal fasciculus modulates the degree of response conflict indexed by N2 in healthy adults. *Brain Res* 1676:1–8.
- Gao R, Peterson EJ, Voytek B (2017a) Inferring synaptic excitation/inhibition balance from field potentials. *Neuroimage* 158:70–78.
- Garyfallidis E, Brett M, Amirbekian B, Rokem A, van der Walt S, Descoteaux M, Nimmo-Smith I, Dipy Contributors (2014) Dipy, a library for the analysis of diffusion MRI data. *Front Neuroinform* 8:8.
- Goldman RI, Stern JM, Engel J Jr, Cohen MS (2002) Simultaneous EEG and fMRI of the alpha rhythm. *Neuroreport* 13:2487–2492.
- Gramfort A, et al. (2013) MEG and EEG data analysis with MNE-python. *Front Neurosci* 7:267.
- Haegens S, Nacher V, Luna R, Romo R, Jensen O (2011)  $\alpha$ -Oscillations in the monkey sensorimotor network influence discrimination performance by rhythmical inhibition of neuronal spiking. *Proc Natl Acad Sci U S A* 108:19377–19382.
- Halgren M, et al. (2019) The generation and propagation of the human alpha rhythm. *Proc Natl Acad Sci U S A* 116:23772–23782.
- Henriques RN, Correia MM, Marralle M, Huber E, Kruper J, Koudoro S, Yeatman JD, Garyfallidis E, Rokem A (2021) Diffusional kurtosis imaging in the diffusion imaging in python project. *Front Hum Neurosci* 15:675433.
- Hindriks R, Woolrich M, Luckhoo H, Joansson M, Mohseni H, Kringelbach ML, Deco G (2015) Role of white-matter pathways in coordinating alpha oscillations in resting visual cortex. *Neuroimage* 106:328–339.
- Hughes SW, Crunelli V (2005) Thalamic mechanisms of EEG alpha rhythms and their pathological implications. *Neuroscientist* 11:357–372.
- Hughes SW, Lörincz M, Cope DW, Blethyn KL, Kékesi KA, Parri HR, Juhász G, Crunelli V (2004) Synchronized oscillations at  $\alpha$  and  $\theta$  frequencies in the lateral geniculate nucleus. *Neuron* 42:253–268.
- Jas M, Engemann DA, Bekhti Y, Raimondo F, Gramfort A (2017) Autoreject: automated artifact rejection for MEG and EEG data. *Neuroimage* 159:417–429.
- Jensen O, Bonnefond M (2013) Prefrontal alpha- and beta-band oscillations are involved in rule selection. *Trends Cogn Sci* 17:10–12.
- Jensen O, Gips B, Bergmann TO, Bonnefond M (2014) Temporal coding organized by coupled alpha and gamma oscillations prioritize visual processing. *Trends Neurosci* 37:357–369.
- Jensen JH, Helpert JA, Ramani A, Lu H, Kaczynski K (2005) Diffusional kurtosis imaging: the quantification of non-Gaussian water diffusion by means of magnetic resonance imaging. *Magn Reson Med* 53:1432–1440.
- Jensen O, Mazaheri A (2010) Shaping functional architecture by oscillatory alpha activity: gating by inhibition. *Front Hum Neurosci* 4:186.
- Jensen O, Pan Y, Frisson S, Wang L (2021) An oscillatory pipelining mechanism supporting previewing during visual exploration and reading. *Trends Cogn Sci* 25:1033–1044.
- Jeurissen B, Leemans A, Tournier J-D, Jones DK, Sijbers J (2013) Investigating the prevalence of complex fiber configurations in white matter tissue with diffusion magnetic resonance imaging. *Hum Brain Mapp* 34:2747–2766.
- Jirsa VK, Haken H (1996) Field theory of electromagnetic brain activity. *Phys Rev Lett* 77:960–963.
- Jirsa VK, Haken H (1997) A derivation of a macroscopic field theory of the brain from the quasi-microscopic neural dynamics. *Physica D* 99:503–526.
- Joliot M, Jobard G, Naveau M, Delcroix N, Petit L, Zago L, Crivello F, Mellet E, Mazoyer B, Tzourio-Mazoyer N (2015) AICHA: an atlas of intrinsic connectivity of homotopic areas. *J Neurosci Methods* 254:46–59.
- Kemmotsu N, Girard HM, Kucukboyaci NE, McEvoy LK, Hagler DJ Jr, Dale AM, Halgren E, McDonald CR (2012) Age-related changes in the neurophysiology of language in adults: relationship to regional cortical thinning and white matter microstructure. *J Neurosci* 32:12204–12213.
- Kruper J, et al. (2021) Evaluating the reliability of human brain white matter tractometry. *Apert Neuro* 1:1–26.
- Lange J, Oostenveld R, Fries P (2013) Reduced occipital alpha power indexes enhanced excitability rather than improved visual perception. *J Neurosci* 33:3212–3220.
- Langer N, Ho EJ, Alexander LM, Xu HY, Jozanovic RK, Henin S, Petroni A, Cohen S, Marcelle ET, Parra LC, Milham MP, Kelly SP (2017) Data descriptor: a resource for assessing information processing in the developing brain using EEG and eye tracking. Available at: [https://academicworks.cuny.edu/cc\\_pubs/567/](https://academicworks.cuny.edu/cc_pubs/567/) (Accessed July 18, 2023).
- Lendner JD, Helfrich RF, Mander BA, Romundstad L, Lin JJ, Walker MP, Larsson PG, Knight RT (2020) An electrophysiological marker of arousal level in humans. *eLife* 9:1–29.
- Liu Z, de Zwart JA, Yao B, van Gelderen P, Kuo L-W, Duyn JH (2012) Finding thalamic BOLD correlates to posterior alpha EEG. *Neuroimage* 63:1060–1069.
- Lobsien D, Ettrich B, Sotiriou K, Classen J, Then Bergh F, Hoffmann K-T (2014) Whole-brain diffusion tensor imaging in correlation to

- visual-evoked potentials in multiple sclerosis: a tract-based spatial statistics analysis. *Am J Neuroradiol* 35:2076–2081.
- Lopes da Silva F (1991) Neural mechanisms underlying brain waves: from neural membranes to networks. *Electroencephalogr Clin Neurophysiol* 79:81–93.
- Lopes Da Silva FH, Storm Van Leeuwen W (1977) The cortical source of the alpha rhythm. *Neurosci Lett* 6:237–241.
- Lopes da Silva FH, van Lierop THMT, Schrijer CF, Storm van Leeuwen W (1973) Organization of thalamic and cortical alpha rhythms: spectra and coherences. *Electroencephalogr Clin Neurophysiol* 35:627–639.
- Lopes da Silva FH, Vos JE, Mooibroek J, van Rotterdam A (1980) Relative contributions of intracortical and thalamo-cortical processes in the generation of alpha rhythms, revealed by partial coherence analysis. *Electroencephalogr Clin Neurophysiol* 50:449–456.
- Lorincz ML, Kékesi KA, Juhász G, Crunelli V, Hughes SW (2009) Temporal framing of thalamic relay-mode firing by phasic inhibition during the alpha rhythm. *Neuron* 63:683–696.
- Lukashevich IP, Sazonova OB (1996) The effect of lesions of different parts of the optic thalamus on the nature of the bioelectrical activity of the human brain. *Zh Vyssh Nerv Deiat Im I P Pavlova* 46:866–874.
- Lunque Laguna PA, Combes AJE, Streffer J, Einstein S, Timmers M, Williams SCR, Dell'Acqua F (2020) Reproducibility, reliability and variability of FA and MD in the older healthy population: a test-retest multiparametric analysis. *Neuroimage Clin* 26:102168.
- Lynch KM, Cabeen RP, Toga AW, Clark KA (2020) Magnitude and timing of major white matter tract maturation from infancy through adolescence with NODDI. *Neuroimage* 212:116672.
- Mathewson KE, Gratton G, Fabiani M, Beck DM, Ro T (2009) To see or not to see: prestimulus alpha phase predicts visual awareness. *J Neurosci* 29:2725–2732.
- Minami S, Oishi H, Takemura H, Amano K (2020) Inter-individual differences in occipital alpha oscillations correlate with white matter tissue properties of the optic radiation. *eNeuro* 7:1–11.
- Mo J, Schroeder CE, Ding M (2011) Attentional modulation of alpha oscillations in macaque inferotemporal cortex. *J Neurosci* 31:878–882.
- Muncy NM, Kimbler A, Hedges-Muncy AM, McMakin DL, Mattfeld AT (2022) General additive models address statistical issues in diffusion MRI: an example with clinically anxious adolescents. *Neuroimage Clin* 33:102937.
- Musall S, von Pföthl V, Rauch A, Logothetis NK, Whittingstall K (2014) Effects of neural synchrony on surface EEG. *Cereb Cortex* 24:1045–1053.
- Nunez PL (2011) Implications of white matter correlates of EEG standing and traveling waves. *Neuroimage* 57:1293–1299.
- Nunez PL, Srinivasan R, Fields RD (2015) EEG functional connectivity, axon delays and white matter disease. *Clin Neurophysiol* 126:110–120.
- Popov T, Szyszka P (2020) Alpha oscillations govern interhemispheric spike timing coordination in the honey bee brain. *Proc Biol Sci* 287:20200115.
- Price D, Cam-CAN, Tyler LK, Neto Henriques R, Campbell KL, Williams N, Treder MS, Taylor JR, Henson RNA (2017) Age-related delay in visual and auditory evoked responses is mediated by white- and gray-matter differences. *Nat Commun* 8:15671.
- Renauld E, Descoteaux M, Bernier M, Garyfallidis E, Whittingstall K (2016) Semi-automatic segmentation of optic radiations and LGN, and their relationship to EEG alpha waves. *PLoS One* 11:e0156436.
- Richie-Halford A, et al. (2022a) An analysis-ready and quality controlled resource for pediatric brain white-matter research. *Sci Data* 9:616.
- Richie-Halford A, Chang K, Gomez T, Hagen M, Rokem A (2023). Tractable: analyzing diffusion MRI tract profiles. R package version 0.0.0.9000, Available at:
- Richie-Halford A, Cieslak M, Ai L, Caffarra S, Covitz S, Franco AR, Karipidis II, Kruper J, Milham M, Avelar-Pereira B (2022b) An analysis-ready and quality controlled resource for pediatric brain white-matter research.
- Salmela-Aro K (2011) Stages of adolescence. In: *Encyclopedia of adolescence* (Brown BB, Prinstein MJ, eds), pp 360–368. London: Academic press.
- Samaha J, Postle BR (2015) The speed of alpha-band oscillations predicts the temporal resolution of visual perception. *Curr Biol* 25:2985–2990.
- Sherbondy AJ, Dougherty RF, Napel S, Wandell BA (2008) Identifying the human optic radiation using diffusion imaging and fiber tractography. *J Vis* 8:12.1–11.
- Shin J, Rowley J, Chowdhury R, Jolicoeur P, Klein D, Grova C, Rosa-Neto P, Kobayashi E (2019) Inferior longitudinal fasciculus' role in visual processing and language comprehension: a combined MEG-DTI study. *Front Neurosci* 13:875.
- Taddei M, Tettamanti M, Zanoni A, Cappa S, Battaglia M (2012) Brain white matter organisation in adolescence is related to childhood cerebral responses to facial expressions and harm avoidance. *Neuroimage* 61:1394–1401.
- Takemura H, Yuasa K, Amano K (2020) Predicting neural response latency of the human early visual cortex from MRI-based tissue measurements of the optic radiation. *eNeuro* 7:1–18.
- Tau GZ, Peterson BS (2010) Normal development of brain circuits. *Neuropsychopharmacology* 35:147–168.
- Tingley D, Yamamoto T, Hirose K, Keele L, Imai K (2014) Mediation: R package for causal mediation analysis. *J Stat Softw* 59:1–38.
- Tootell RBH, Tsao D, Vanduffel W (2003) Neuroimaging weighs in: humans meet macaques in “primate” visual cortex. *J Neurosci* 23:3981–3989.
- Traub RD, Hawkins K, Adams NE, Hall SP, Simon A, Whittington MA (2020) Layer 4 pyramidal neuron dendritic bursting underlies a post-stimulus visual cortical alpha rhythm. *Commun Biol* 3:230.
- Tröndle M, Popov T, Dziemian S, Langer N (2022) Decomposing the role of alpha oscillations during brain maturation. *eLife* 11:e77571.
- Uddin MN, Figley TD, Solar KG, Shatil AS, Figley CR (2019) Comparisons between multi-component myelin water fraction, T1w/T2w ratio, and diffusion tensor imaging measures in healthy human brain structures. *Sci Rep* 9:2500.
- Uhlhaas PJ, Roux F, Rodriguez E, Rotarska-Jagiela A, Singer W (2010) Neural synchrony and the development of cortical networks. *Trends Cogn Sci* 14:72–80.
- Valdés-Hernández PA, Ojeda-González A, Martínez-Montes E, Lage-Castellanos A, Virués-Alba T, Valdés-Urrutia L, Valdes-Sosa PA (2010) White matter architecture rather than cortical surface area correlates with the EEG alpha rhythm. *Neuroimage* 49:2328–2339.
- Van Diepen RM, Foxe JJ, Mazaheri A (2019) The functional role of alpha-band activity in attentional processing: the current zeitgeist and future outlook. *Curr Opin Psychol* 29:229–238.
- Van Dijk H, Schoffelen J-M, Oostenveld R, Jensen O (2008) Prestimulus oscillatory activity in the alpha band predicts visual discrimination ability. *J Neurosci* 28:1816–1823.
- Van Essen DC, Smith SM, Barch DM, Behrens TEJ, Yacoub E, Ugurbil K, WU-Minn HCP Consortium (2013) The WU-minn human connectome project: an overview. *Neuroimage* 80:62–79.
- Vijayan S, Kopell NJ (2012) Thalamic model of awake alpha oscillations and implications for stimulus processing. *Proc Natl Acad Sci U S A* 109:18553–18558.
- Wagenmakers E-J, Sarafoglou A, Aczel B (2022) One statistical analysis must not rule them all. *Nature* 605:423–425.
- Westlye LT, Walhovd KB, Bjørnerud A, Due-Tønnessen P, Fjell AM (2009) Error-related negativity is mediated by fractional anisotropy in the posterior cingulate gyrus—a study combining diffusion tensor imaging and electrophysiology in healthy adults. *Cereb Cortex* 19:293–304.
- Whitford TJ, Kubicki M, Ghorashi S, Schneiderman JS, Hawley KJ, McCarley RW, Shenton ME, Spencer KM (2011) Predicting inter-hemispheric transfer time from the diffusion properties of the corpus callosum in healthy individuals and schizophrenia patients: a combined ERP and DTI study. *Neuroimage* 54:2318–2329.
- Wiecki TV, Sofer I, Frank MJ (2013) HDDM: hierarchical Bayesian estimation of the drift-diffusion model in Python. *Front Neuroinform* 7:14.
- Yeatman JD, Dougherty RF, Myall NJ, Wandell BA, Feldman HM (2012) Tract profiles of white matter properties: automating fiber-tract quantification. *PLoS One* 7:e49790.